Observation of quantum-classical correspondence from high-order transverse patterns

Y. F. Chen,* Y. P. Lan, and K. F. Huang
Department of Electrophysics, National Chiao Tung University, Hsinchu, Taiwan, Republic of China
(Received 23 October 2002; published 6 October 2003)

We experimentally observe the formation of high-order transverse patterns in a laser resonator with a high degree of frequency degeneracy. It is found that the transverse patterns are well localized on the *Lissajous* orbits. The connection between the wave functions and the classical periodic orbits is analytically constructed by using the representation of SU(2) coherent states. With this connection, the observed transverse patterns are reconstructed very well. The nice reconstruction suggests that the laser resonators can be deliberately designed to attain a more thorough understanding of the quantum-classical connection.

DOI: 10.1103/PhysRevA.68.043803 PACS number(s): 42.60.Jf, 03.65.−w, 05.45.Mt

It is well known that the paraxial wave equation for the spherical laser resonators has the identical form with the Schrödinger equation for the two-dimensional (2D) harmonic oscillator [1,2]. The eigenfunction of the 2D quantum harmonic oscillator can be analytically expressed as a Hermite-Gaussian function with Cartesian symmetry (x,y) or a Laguerre-Gaussian function with cylindrical symmetry (r,ϕ) [1–3]. Since the functional forms of the 2D quantum oscillator and the spherical resonators are similar, the higher transverse modes of the spherical resonators can be in terms of Hermite-Gaussian (HG) modes or Laguerre-Gaussian (LG) modes.

The wave functions of HG mode native to a spherical resonator are given by

$$\Phi_{m,n}^{(\mathrm{HG})}(x,y;\varpi_o)=\frac{1}{\sqrt{2^{m+n-1}\pi m!n!}}\frac{1}{\varpi_o}H_m\left(\frac{\sqrt{2}x}{\varpi_o}\right)H_n\left(\frac{\sqrt{2}y}{\varpi_o}\right)\times\exp\left[-\frac{(x^2+y^2)}{\varpi_o^2}\right], \tag{1}$$

with the resonance frequencies

$$\nu_{l,m,n}=l(\Delta\nu_L)+(m+n+1)(\Delta\nu_t), \tag{2}$$

where $H_n(\cdot)$ is a Hermite polynomial of order n, ϖ_o is the laser beam waist, l is the longitudinal mode index, m and n are the transverse mode indices, $\Delta\nu_L$ is the longitudinal mode spacing, and $\Delta\nu_T$ is the transverse mode spacing. For a plano-concave resonator, as shown in Fig. 1, the transverse mode spacing is given by

$$\Delta\nu_T=\Delta\nu_L\left[\frac{1}{\pi}\cos^{-1}\left(\sqrt{1-\frac{d}{R}}\right)\right], \tag{3}$$

where d is the cavity length and R is the radius of curvature of the output coupler. Recently, we use a doughnut pump profile to generate the $\mathrm{LG}_{0\pm N}$ modes in an *a*-cut Nd:YVO_4 laser [4] and to generate the elliptical modes in a *c*-cut Nd:YVO_4 laser [5]. The emission from *a*-cut Nd:YVO_4 crystals is linearly polarized, whereas the emission is usually a random polarization for *c*-cut crystals. The polarization property is the main difference between *a*-cut and *c*-cut crystals. Therefore, when a linear polarized emission is desired, *a*-cut crystals are used. The $\mathrm{LG}_{0\pm N}$ modes are formed by the superposition of the degenerate HG eigenmodes $\Phi_{K,N-K}^{(\mathrm{HG})}(x,y;\varpi_o)$, where $K=0,1,2,\ldots,N$ [3]

$$\Phi_{0,\pm N}^{(\mathrm{LG})}(x,y;\varpi)=2^{-N/2}\sum_{K=0}^{N}\binom{N}{K}^{1/2}(\pm i)^K\Phi_{K,N-k}^{(\mathrm{HG})}(x,y;\varpi_o). \tag{4}$$

To generate $\mathrm{LG}_{0\pm N}$ modes we setup the resonator length to be as short as possible for reaching single-longitudinal mode operation and $\Delta\nu_L\gg\Delta\nu_T$.

As indicated in Eq. (3), adjusting the cavity length d may result in the ratio $\Delta\nu_L/\Delta\nu_T$ to be an integer S. These cavity configurations constitute a high degree of frequency degeneracy. From Eq. (2) it can be seen that lowering (raising) the longitudinal mode index l by K, while simultaneously raising (lowering) the sum of the transverse mode indices $n+m$ by $S\times K$, will leave the frequency unaltered. It has been shown that configurations with a high degree of frequency degeneracy allow closed geometric trajectories [6]. So far, the transverse modes suited in a frequency degenerate cavity are focused on one dimension [7]. Here we use the cavity shown

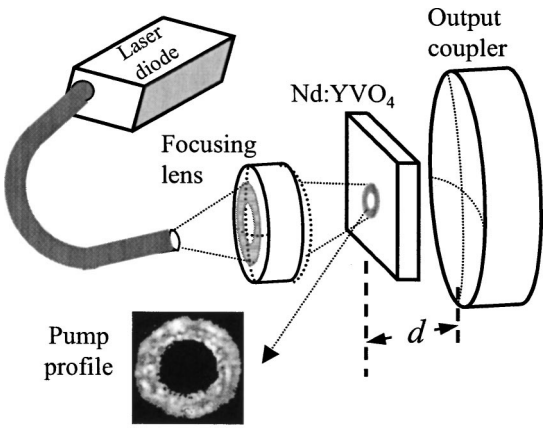

FIG. 1. Schematic of a fiber-coupled diode-end-pumped microchip laser; a typical pump profile of a fiber-coupled laser diode away from the focal plane; the cavity length d is set at $\Delta\nu_L/\Delta\nu_T=3$.

*Email address: yfchen@cc.nctu.edu.tw

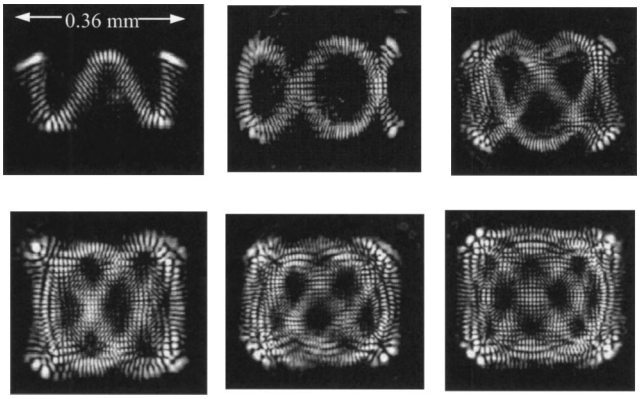

FIG. 2. Experimental results for the typical transverse patterns observed in a cavity length near $\Delta\nu_L/\Delta\nu_T=3$.

in Fig. 1 to investigate 2D transverse modes in a frequency degenerate cavity with an *a*-cut Nd:YVO_4 microchip laser. The radius of curvature of the output coupler is 10 mm. The pump radius on the crystal is controlled to be around $\varpi_p = 0.16-0.22$ mm. Experimental measurement reveals that the thickness of the pump ring can be approximately expressed as $\Delta\varpi_p = 0.025 + 0.16\varpi_p$ (mm). In other words, the thickness of the pump profile relatively increases with increasing the pump radius. The fundamental mode size in the present cavity is $\varpi_o \approx 0.04$ mm. From the formula $\mathrm{Fr} = \omega_p^2/(\pi\omega_0^2)$, the Fresnel number can be estimated to be 5–10. Since the emission from an *a*-cut crystal is naturally linearly polarized, the experimental pattern is a pure scalar field. Slightly adjusting the cavity length in the vicinity of $\Delta\nu_L/\Delta\nu_T=3$ and controlling the pump spot size, several typical sharp patterns on the concave mirror are obtained and shown in Fig. 2. The sharp patterns outside the resonator are found to be preserved in free-space propagation. The preservation of the experimental patterns consists of the property that HG modes remain HG field patterns as they propagate. The incident angle of the pump beam is controlled to be within $\pm 5°$ with respect to the longitudinal axis. The critical points to obtain a locked pattern consist in the adjustment of the cavity length and the use of the doughnut pump profile. The fine modification of the pump angle can further enhance the sharp patterns, however, it is very difficult to precisely define the optimal incident angle for each pattern. Although each different sharp pattern is obtained at a different cavity length, the change of the cavity lengths is rather short. The difference between the cavity lengths of two sharp patterns is approximately 30 μm. The difference of the cavity lengths for different sharp patterns mainly arises from the fact that the effective cavity length depends on the order of the transverse mode, even though the dependence is very weak. Specifically there is unavoidable astigmatism in the present cavity because of the thermal lensing effect and anisotropic properties of the gain medium. Astigmatism-induced splitting of the two degenerate mode frequencies can lead to a significant influence on laser dynamics [4]. Here we believe that the inevitable astigmatism plays an important role not only for the dependence of the effective cavity length on the transverse order but also for the origin of the symmetry breaking of the present experiment. The range of the cavity length for each sharp pattern to be structure stable is around 10 μm. When the cavity length does not meet the range of the locking modes, the transverse pattern is usually irregular and vague. It can be seen that the observed sharp patterns are completely unlike a HG or LG mode. Interestingly, these patterns are well localized on the *Lissajous* figures that are classical periodic orbits for a 2D anisotropic harmonic oscillator with commensurate frequencies. The measurement of the optical spectrum shows that all observed patterns are single frequency emissions. In other words, the transverse pattern formation is a spontaneous process of cooperative frequency locking [8]. However, it is worthwhile to note that the frequency locking of the present patterns is among different transverse order with the help of different longitudinal order.

To explain the observed patterns, it is essential to know how the wave functions can be associated with the classical trajectories for a 2D harmonic oscillator. Here we use the representation of the SU(2) coherent state to make a connection between the wave functions and the classical trajectories in a 2D anisotropic oscillator with commensurate frequencies. The Hamiltonian for a 2D quantum harmonic oscillator is generally given by

$$H=\frac{-\hbar^2}{2m_x}\frac{\partial^2}{\partial x^2}+\frac{-\hbar^2}{2m_y}\frac{\partial^2}{\partial y^2}+\frac{m_x\omega_x^2x^2}{2}+\frac{m_y\omega_y^2y^2}{2}. \quad (5)$$

The eigenfunctions of Eq. (5) can be expressed as

$$\Phi_{m,n}(x,y;\varpi_x,\varpi_y)=\frac{1}{\sqrt{2^{m+n-1}\pi m!n!}}\frac{1}{\sqrt{\varpi_x\varpi_y}} \times H_m\left(\frac{\sqrt{2}x}{\varpi_x}\right)H_n\left(\frac{\sqrt{2}y}{\varpi_y}\right) \times\exp\left[-\left(\frac{x^2}{\varpi_x^2}+\frac{y^2}{\varpi_y^2}\right)\right], \quad (6)$$

where $\varpi_x=\sqrt{2\hbar/(m_x\omega_x)}$ and $\varpi_y=\sqrt{2\hbar/(m_y\omega_y)}$. The eigenvalues associated with the eigenfunctions $\Phi_{m,n}(x,y;\varpi_x,\varpi_y)$ are given by

$$E_{m,n}=\left(m+\frac{1}{2}\right)\hbar\omega_x+\left(n+\frac{1}{2}\right)\hbar\omega_y. \quad (7)$$

As is well known, the classical trajectory for 2D anisotropic harmonic oscillator with commensurate frequencies is a periodic orbit, called a *Lissajous* figure [9]. However, the conventional eigenstates $\Phi_{m,n}(x,y;\varpi_x,\varpi_y)$ do not manifest the characteristics of classical periodic orbits even in the correspondence limit of large quantum numbers.

Recently, the wave functions associated with the classical elliptical trajectories in a 2D isotropic harmonic oscillator have been analytically constructed by using the representation of SU(2) coherent states [10,11]. Mathematically, the SU(2) coherent states is a superposition of degenerate eigenstates. Here we find that the wave functions related to the *Lissajous* figures can be constructed by coherent states similar to the SU(2) representation. Consider a 2D anisotropic harmonic oscillator with frequencies in the ratio $\omega_x:\omega_y=q:p$, where p and q are integers. The eigenvalues can be rewritten in the form

$$E_{m,n}=\left[\left(m+\frac{1}{2}\right)q+\left(n+\frac{1}{2}\right)p\right]\hbar\omega, \tag{8}$$

where ω is the common factor of the frequencies ϖ_x and ϖ_y. For $q:p$ anisotropic quantum oscillators, it is explicit that a family of the eigenstates $\Phi_{pK,q(N-K)}(x,y;\varpi_x,\varpi_y)$ with $K=0,1,2,\ldots,N$ are degenerate for a given index N and the eigenvalue of these eigenstates is given by $E_N=[pqN+(p+q)/2]\hbar\omega$. As in the Schwinger representation of the SU(2) algebra, the coherent state for $q:p$ anisotropic quantum oscillators is given by

$$\Psi_N^{p,q}(x,y;\varpi_x,\varpi_y,\tau)=\frac{1}{(1+|\tau|^2)^{N/2}}\sum_{K=0}^{N}\binom{N}{K}^{1/2}\times\tau^K\Phi_{pK,q(N-k)}(x,y;\varpi_x,\varpi_y), \tag{9}$$

where the parameter τ is, in general, complex and $|\tau|^2$ is approximately the ratio of the mean energies in the x and y axes. With the SU(2) coherent state in Eq. (9), the mean energies in the x and y axes are derived to be

$$E_{N,x}=\left[pqN\left(\frac{|\tau|^2}{1+|\tau|^2}\right)+\frac{q}{2}\right]\hbar\omega,$$

$$E_{N,y}=\left[pqN\left(\frac{1}{1+|\tau|^2}\right)+\frac{p}{2}\right]\hbar\omega. \tag{10}$$

It can be found that $E_N=E_{N,x}+E_{N,y}$ and the ratio $E_{N,x}/E_{N,y}$ approaches $|\tau|^2$ for $N\gg1$.

For making a connection with the classical periodic orbits, it is convenient to express the parameter τ as the polar representation, i.e., $\tau=A\exp(i\phi)$. In terms of A and ϕ, the coherent state $\Psi_N^{p,q}(x,y;\varpi_x,\varpi_y,Ae^{i\phi})$ can be associated with the *Lissajous* figures,

$$x(t)=\sqrt{2\langle x^2\rangle}\cos\left(q\omega t-\frac{\phi}{p}\right),$$

$$y(t)=\sqrt{2\langle y^2\rangle}\cos(p\omega t), \tag{11}$$

where

$$\langle x^{2\prime}\rangle=\left(\frac{A^2}{1+A^2}pN+\frac{1}{2}\right)\frac{\varpi_x^2}{2},$$

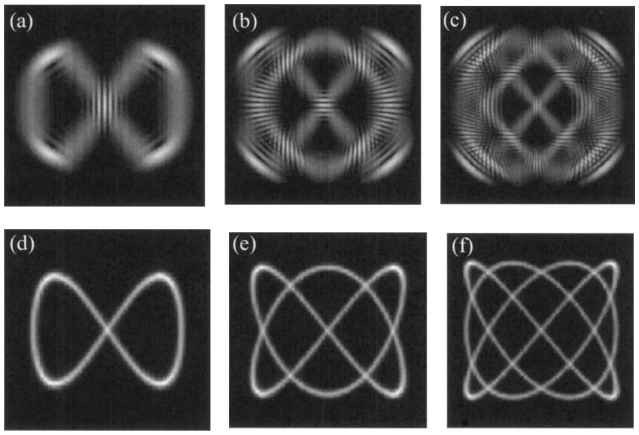

FIG. 3. A comparison between the coherent states and the classical *Lissajous* periodic orbits for $p:q$ to be 2:1, 3:2, and 4:3. (a)–(c) The coherent states calculated with Eq. (9) and $\tau=\exp(i\pi/2)$ and $N=30$. (d)–(f) The coherent states calculated with Eqs. (11) and (12) and $A=1$, $\phi=\pi/2$, and $\varpi_x=\varpi_y$.

$$\langle y^2\rangle=\left(\frac{1}{1+A^2}qN+\frac{1}{2}\right)\frac{\varpi_y^2}{2}. \tag{12}$$

Note that $\langle x^2\rangle$ and $\langle y^2\rangle$ are, respectively, the expectation values of x^2 and y^2 for the coherent state $\Psi_N^{p,q}(x,y;\varpi_x,\varpi_y,Ae^{i\phi})$. Figure 3 shows a comparison between the SU(2) coherent states and the classical Lissajous figures for the frequency ratio of 2:1, 3:2, and 4:3 with $A=1$, $\phi=\pi/2$, $\varpi_x=\varpi_y$, and $N=30$. It can be seen that the distributions of $|\Psi_N^{p,q}(x,y;\varpi_x,\varpi_y,Ae^{i\phi})|^2$ are in good agreement with the classical periodic orbits. Moreover, the behavior of $|\Psi_N^{p,q}(x,y;\varpi_x,\varpi_y,Ae^{i\phi})|^2$ illustrates geometrically Bohr's correspondence principle: the velocity of the classical particle is at a minimum at the apogees of the motion, and therefore the probability density has a peak at these points.

Although the number of eigenstates used in the coherent state $\Psi_N^{p,q}(x,y;\varpi_x,\varpi_y,Ae^{i\phi})$ is $N+1$, the number of dominant eigenstates for wave localization is rather small for high-order states. To manifest the efficiency of wave localization, we modify $\Psi_N^{p,q}(x,y;\varpi_x,\varpi_y,Ae^{i\phi})$ to define a partially coherent state as

$$\Psi_{N,M}^{p,q}(x,y;\varpi_x,\varpi_y,Ae^{i\phi})=\left[\sum_{K=J}^{N-J}\binom{N}{K}A^2\right]^{-1/2}\left[\sum_{K=J}^{N-J}\binom{N}{K}^{1/2}A^Ke^{iK\phi}\times\Phi_{pK,q(N-K)}(x,y;\varpi_x,\varpi_y)\right], \tag{13}$$

where the index $M=N-2J+1$ represents the number of eigenstates used in the state $\Psi_{N,M}^{p,q}(x,y;\varpi_x,\varpi_y,Ae^{i\phi})$.

Numerical analyses reveal that the transverse pattern shown in Fig. 2 can be nicely explained by the partially coherent state in Eq. (13). As mentioned earlier, the formation of the observed patterns is a cooperative frequency locking among different transverse orders with the help of different longitudinal orders. For a cavity near $\Delta\nu_L/\Delta\nu_T=3$, the

family of the transverse modes $\Phi^{(\mathrm{HG})}_{pK,q(N-K)}(x,y;\varpi_o)$ with a given index N can be frequency locked by a different longitudinal index $l=L\mp K$ with a given index L, where $K=0,1,2,...,N$ and $p-q=\pm 3$. Substituting $m=pK$, $n=q(N-K)$, $l=L\mp K$, $p-q=\pm 3$, and $\Delta\nu_L/\Delta\nu_T=3$ into Eq. (2), the laser frequency of the family $\Phi^{(\mathrm{HG})}_{pK,q(N-K)}(x,y;\varpi_o)$ can be found to be $\nu_{L,N}=L(\Delta\nu_L)+(qN+1)(\Delta\nu_T)$ independent of K. From the numerical analysis, the transverse patterns shown in Fig. 2 are found to be associated with the partially coherent states in Eq. (13) with $A=1$ and $\phi=0$. In other words, the wave functions related to the observed patterns can be in terms of HG modes as

$$U^{p,q}_{N,M}(x,y)=\left[\sum_{K=J}^{N-J}\binom{N}{K}\right]^{-1/2}\left[\sum_{K=J}^{N-J}\binom{N}{K}^{1/2}\times\Phi^{(\mathrm{HG})}_{pK,q(N-K)}(x,y;\varpi_o)\right] \tag{14}$$

with $p-q=\pm 3$. Note that for a spherical cavity, the transverse components of the resonance frequencies are not degenerate for each eigenstate in Eq. (14) except for $p=q$. For the Kth eigenstate of the coherent state $U^{p,q}_{N,M}(x,y)$, the transverse components of the resonance frequencies are $[qN+1+(p-q)K]\Delta\nu_T$. If the condition of $p-q=\pm 3$ is satisfied, then the frequency of each eigenstate in the coherent state $U^{p,q}_{N,M}(x,y)$ can be possibly locked with the help of different longitudinal component of $(L\mp K)\Delta\nu_L$ because of $\Delta\nu_L/\Delta\nu_T=3$. To be brief, the formation of the present transverse patterns is a spontaneous frequency locking in the 2+1 dimension, not a pure transverse mode locking. Figure 4 shows the numerically reconstructed patterns for the results shown in Fig. 2, calculated with Eq. (14) for several cases of $p-q=\pm 3$. It is clear that only 3–5 eigenstates are already sufficient to localize the wave patterns on the classical trajectories, even for high-order periodic orbits. The present analysis indicates that the wave function obtained as a linear superposition of a few degenerate eigenstates can provide a more physical description of a phenomenon than the true eigenstates in mesoscopic systems [12]. The good agreement between the experimental and reconstructed patterns confirms that the interrelation between wave optics and geometrical optics is somewhat similar to that between quantum and classical mechanics. Such an analogy enables us to employ quantum theory in analyzing the formation of high-order laser transverse modes.

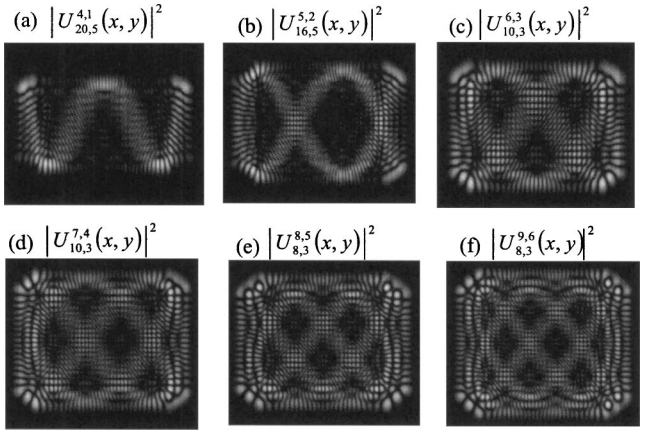

FIG. 4. The numerically reconstructed patterns for the results shown in Fig. 2, calculated with Eq. (14). (a) $|U^{4,1}_{20,5}(x,y)|^2$; (b) $|U^{5,2}_{16,5}(x,y)|^2$; (c) $|U^{6,3}_{10,3}(x,y)|^2$; (d) $|U^{7,4}_{10,3}(x,y)|^2$; (e) $|U^{8,5}_{8,3}(x,y)|^2$; (f) $|U^{9,6}_{8,3}(x,y)|^2$.

In conclusion, we have used the representation of the SU(2) coherent state to make a connection between the wave functions and the classical trajectories in a 2D anisotropic oscillator with commensurate frequencies. With the analytical wave function, the experimental transverse patterns associated with the *Lissajous* trajectories can be explained very well. The nice explanation suggests that the laser resonators with an identical functional form can be used to attain a more thorough understanding of the quantum-classical connection. It is worthwhile to mention that a similar phenomenon is found in a nonintegrable classical system; the wave patterns of the eigenstates are usually concentrated along unstable periodic orbits instead of being randomly distributed [13–15]. In addition, there are some striking phenomena in open quantum ballistic cavities associated with the wave functions in terms of classical periodic orbits [16–18]. Therefore, to construct the connection between the wave functions and classical periodic trajectories is not only useful for explaining the present transverse patterns but also helpful for understanding quantum-classical correspondence as well as the quantum transport in mesoscopic systems. Recently, Doya *et al.* [19,20] have introduced the paraxial approximation to establish an analogy between light propagation along a multimode fiber and quantum confined systems. We believe that these analogies will continue to be exploited for understanding the physics of mesoscopic systems.

The authors thank the National Science Council for financially supporting this research under Contract No. NSC-91-2112-M-009-030.

[1] H. A. Haus, *Waves and Fields in Optoelectronics* (Prentice-Hall, Englewood Cliffs, NJ, 1984).
[2] A. E. Siegman, *Lasers* (University Science Books, Mill Valley, CA, 1986).
[3] L. Allen, M. W. Beijersbergen, R. J. C. Spreeuw, and J. P. Woerdman, Phys. Rev. A **45**, 8185 (1992).
[4] Y. F. Chen and Y. P. Lan, Phys. Rev. A **63**, 063807 (2001).
[5] Y. F. Chen and Y. P. Lan, Phys. Rev. A **66**, 053812 (2002).
[6] I. A. Ramsay and J. J. Degnan, Appl. Opt. **9**, 385 (1970).
[7] J. Dingjan, M. P. van Exter, and J. P. Woerdman, Opt. Commun. **188**, 345 (2001).
[8] L. A. Lugiato, C. Oldano, and L. M. Narducci, J. Opt. Soc. Am. B **5**, 879 (1988).
[9] H. Goldstein, *Classical Mechanics*, 2nd ed. (Addison-Wesley, Reading, MA, 1980).
[10] S. De Bièvre, J. Phys. A **25**, 3399 (1992).

[11] J. Pollet, O. Méplan, and C. Gignoux, J. Phys. A **28**, 7282 (1995).
[12] R. Narevich, R. E. Prange, and O. Zaitsev, Phys. Rev. E **62**, 2046 (2000).
[13] M. V. Berry, Proc. R. Soc. London, Ser. A **423**, 219 (1989).
[14] E. J. Heller, Phys. Rev. Lett. **53**, 1515 (1984).
[15] F. Simonotti, E. Vergini, and M. Saraceno, Phys. Rev. E **56**, 3859 (1997).
[16] R. Akis and D. K. Ferry, Phys. Rev. B **59**, 7529 (1999).
[17] I. V. Zozoulenko and K. F. Berggren, Phys. Rev. B **56**, 6931 (1997).
[18] Y. H. Kim, M. Barth, H. J. Stöckmann, and J. P. Bird, Phys. Rev. B **65**, 165317 (2002).
[19] V. Doya, O. Legrand, F. Mortessagne, and C. Miniatura, Phys. Rev. Lett. **88**, 014102 (2002).
[20] V. Doya, O. Legrand, F. Mortessagne, and C. Miniatura, Phys. Rev. E **65**, 056223 (2002).